A Unified Simplicial Model for Mixed-Dimensional and Non-Manifold Deformable Elastic Objects

JUMYUNG CHANG, University of Waterloo, Canada
FANG DA, Waymo, USA
EITAN GRINSPUN, Columbia University, USA
CHRISTOPHER BATTY, University of Waterloo, Canada

We present a unified method to simulate deformable elastic bodies consisting of mixed-dimensional components represented with potentially non-manifold simplicial meshes. Building on well-known simplicial rod, shell, and solid models for elastic continua, we categorize and define a comprehensive palette expressing all possible constraints and elastic energies for stiff and flexible connections between the 1D, 2D, and 3D components of a single conforming simplicial mesh. This palette consists of three categories: *point connections*, in which simplices meet at a single vertex around which they may twist and bend; *curve connections* in which simplices share an edge around which they may rotate (bend) relative to one another; and *surface connections*, in which a shell is embedded on or into a solid. To define elastic behaviors across non-manifold point connections, we adapt and apply parallel transport concepts from elastic rods. To address discontinuous forces that would otherwise arise when large accumulated relative rotations wrap around in the space of angles, we develop an incremental angle-update strategy. Our method provides a conceptually simple, flexible, and highly expressive framework for designing complex elastic objects, by modeling the geometry with a single simplicial mesh and decorating its elements with appropriate physical models (rod, shell, solid) and connection types (point, curve, surface). We demonstrate a diverse set of possible interactions achievable with our method, through technical and application examples, including scenes featuring complex aquatic creatures, children's toys, and umbrellas.

CCS Concepts: • **Computing methodologies → Physical simulation**.

Additional Key Words and Phrases: unified, mixed-dimensional, non-manifold, elastic

ACM Reference Format:
Jumyung Chang, Fang Da, Eitan Grinspun, and Christopher Batty. 2019. A Unified Simplicial Model for Mixed-Dimensional and Non-Manifold Deformable Elastic Objects. *Proc. ACM Comput. Graph. Interact. Tech.* 2, 2, Article 11 (July 2019), 18 pages. https://doi.org/10.1145/3340252

1 INTRODUCTION

Most numerical methods for elastic deformable bodies in computer graphics have focused on objects that exhibit a single uniform type or effective dimensionality: 1D rods, 2D shells, or 3D volumetric solids. However, many common objects possess either *non-manifold* connections between parts of possibly differing dimensions, or *embedded* features where a lower dimensional object passes through a higher-dimensional one. Examples include wires or rods threaded through tents, kites,

Authors' addresses: Jumyung Chang, j48chang@uwaterloo.ca, University of Waterloo, Canada; Fang Da, freeman.dafang@gmail.com, Waymo, USA; Eitan Grinspun, eitan@cs.columbia.edu, Columbia University, USA; Christopher Batty, christopher.batty@uwaterloo.ca, University of Waterloo, Canada.

2577-6193/2019/7-ART11 $15.00
https://doi.org/10.1145/3340252

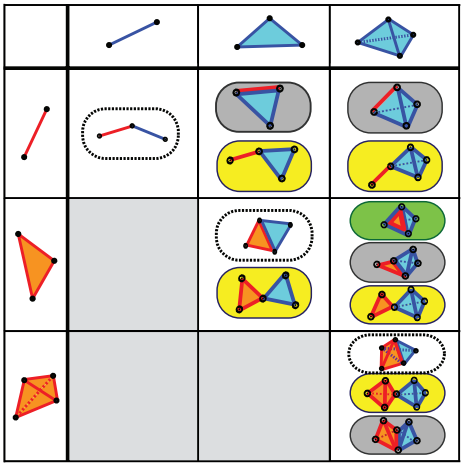

Fig. 1. The set of possible connections among elastic models in a general 3D simplicial mesh. Dashed: single-type. Yellow: shared vertex. Grey: shared edge. Green: shared face. (The connections in the grayed-out cells have been left blank as they are identical to their symmetric counterparts in the top-right.)

or umbrellas; molded rubber and plastic objects composed of smoothly connected components of varying shape and thickness; tendons embedded in flesh or skin wrapped around muscle; and sandwich-structured composites, in which volumes of a soft low-density material are sandwiched between sheets of a stiffer material like aluminum.

Our aim is to characterize and develop a comprehensive palette of mixed-dimensional and/or non-manifold connection types for such elastic objects represented by a single conforming simplicial mesh. We interpret *conforming* to mean that two components are connected exactly along shared simplices (i.e., shared vertices, edges, and/or faces). Figure 1 catalogs all the basic pairwise manifold and non-manifold connections that can arise on such a mesh; these can also be "stacked" to handle higher valence connections.

To express the deformation of components of a particular dimensionality, we leverage existing models. Specifically, we adopt Bergou's (time-parallel) discrete elastic rods [Bergou et al. 2010], Grinspun's discrete shells with hinge-based bending [Grinspun et al. 2003] and linear elastic stretching [Gingold et al. 2004], and St. Venant-Kirchhoff tetrahedral elastic solids [O'Brien and Hodgins 1999]. Other choices are possible, but these are well-studied, widely adopted, and provide a balance of accuracy, simplicity, and efficiency.

While the space of possible connections is large (Figure 1) we distinguish three families: *point (vertex) connections*, *curve (edge) connections*, including rods embedded into shells and solids, and *surface (face) connections*, of which a shell embedded in a solid is the only example. This categorization reduces the conceptual and implementation complexity of methodically developing a unified model. For each case, we describe both hard constraints and soft elastic joints by constructing appropriate reference coordinate frames and measuring deformations in the available modes. We emphasize the elastic case for its greater expressivity.

Our primary contribution is the design of a unified framework for arbitrary simplicial deformable objects. The design of appropriate forces hinges on the ability to perform accurate comparisons between neighboring simplices' orientations, and two enabling technical contributions are particularly critical. First, we argue that joints in elastic rods provide a natural analog for non-manifold point connections. We therefore expand the application of parallel transport from rods to the task

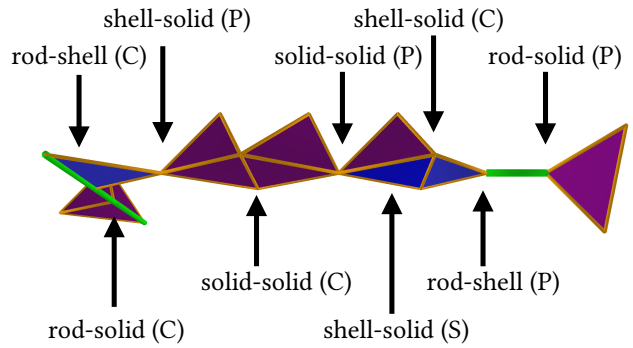

Fig. 2. A simplicial object decorated with many connection types. Purple indicates solid tetrahedra, blue indicates shell triangles, and green indicates rod edges. (P), (C), and (S) mean Point, Curve, and Surface connection, respectively.

of measuring relative deviation in general simplices' reference frames. Second, we observe that large accumulated rotations can lead to sudden spurious jumps in potential energy at point or curve connections when relative angle deviations wrap around in the space of angles. We propose a new incremental angle-update strategy that resolves this issue.

By augmenting standard single-dimensional models with these new capabilities and making judicious design choices, we assemble a comprehensive system for animating simplicial deformable objects. An end-user need only model an object's non-manifold and/or mixed-dimensional geometric mesh and specify its behavior by decorating simplices with model (rod, shell, solid) and connection types. This provides a simple, flexible, and powerful paradigm for modeling diverse deformable objects, which we demonstrate in a variety of application scenarios.

2 RELATED WORK

2.1 Unified non-manifold elastic models

Autodesk's Nucleus platform [Stam 2009] and position-based dynamics [Macklin et al. 2014; Müller and Chentanez 2011; Müller et al. 2007] are the approaches most conceptually similar to ours. They use non-manifold mesh structures augmented with various constraints and/or shape-matching mechanisms to approximate elastic deformations of objects, including rods [Kugelstadt and Schömer 2016; Umetani et al. 2014]; however, they place a reduced emphasis on accuracy compared to the standard continuum mechanics-based approaches that we build upon, and they do not consider elastic bending and twisting at point connections outside the context of pure rods.

Dispensing with an explicit mesh, Martin et al. [2010] proposed a meshless elastic model known as *elastons*. This approach can model continuous elastic bodies, but it is quite complex, is slower than the classic single-type models we build on, and does not address the more general connections and embeddings we consider. Specifically, the elastons model assumes a smooth body of material, whereas our method supports (1) singular point or segment connections with stiffness independent of the connected materials, and (2) embedded structures that allow sharp jumps in stiffness and the ability to disable twisting and/or bending coupling at connections. These can straightforwardly support diverse behaviors for the same geometry (e.g., see our frisbee, toy tunnel, and sandwich composite examples in Figures 13, 14, 16.)

Moreover, the computational overhead of the mesh-free setting generally exceeds that of existing mesh-based alternatives. A more efficient alternative was proposed by Faure, Gilles, and co-workers [Faure et al. 2011; Gilles et al. 2011], which assigns sparse local coordinate frames to points on

the object and uses modified shape functions to construct a continuum mechanics formulation for elasticity. However, this method assumes a volumetric representation of the solid and does not consider rods and shells.

Zhu et al. [2015; 2014] explored the simulation of liquids on non-manifold simplicial meshes. Our work is distinct in that we focus on purely elastic solids rather than fluids. In addition, their lower-dimensional models (i.e., threads and sheets) neglect bending and twisting effects altogether, which play a critical role in the distinctive behaviors of elastica.

2.2 Non-manifold single type models

Spillmann and Teschner [2009] generalized their CoRDe elastic rod model to non-manifold (T-junction) rod configurations to represent Cosserat nets, and Bertails et al. [2006] used non-manifold joints within the super-helices model for branching tree structures. Pérez et al. [2015] used the notion of a connection edge, which acts as a counterpart of an edge representing all the other edges at a point connection. Similarly, Cirak and Long [2011] considered non-manifold shells in which multiple surfaces share an edge or sequence of edges. These higher-valence connections can be handled by our framework, but are not our primary focus.

2.3 Specialized elastic model coupling

Instances of mixed-dimensional interactions, similar in spirit to our work, have been considered in a number of special cases. Li et al. [2014] used impulses to couple cloth and rods to model an umbrella. Chentanez et al. [2009] modeled prostate brachytherapy by coupling embedded elastic rod-based needles to a tetrahedral solid with Lagrange multipliers that allow sliding. Rémillard and Kry [2013] coupled a much higher resolution shell-based skin model to a lower-resolution volumetric simulation to accurately model skin wrinkling effects. Bergou et al. [2008] used Lagrange multipliers to affix a rigid body to the end of a rod with matching orientation. The position-based rod model of Umetani et al. [2014] supports attaching a rod's endpoint to frames, triangles, or rigid bodies. Xu et al. [2018] used equality constraints on the twisting angles to connect different pairs of wire pieces. Pérez et al. [2017] proposed a computational design framework for Kirchhoff-Plateau surfaces using a cloth model augmented with elastic rods embedded in the plane of the cloth. We aim to develop a more broadly applicable unified framework. In engineering, so-called joint or interface elements have been proposed for finite element methods to connect different materials across interfaces, often for shell-shell or solid-shell surface contacts (similar to our embedded models). For example, this approach has been used in geomechanics for modeling joints or fractures in rock structures [Beer 1985; Schellekens and De Borst 1993].

2.4 Constraint-based coupling

We assume that the elastic object to be modeled consists of a single conforming simplicial mesh. A typical alternative is to model each single-dimensional component in isolation and introduce specialized position and/or orientation constraints to tie components back together in a desired fashion; such constraints could be enforced by either Lagrange multipliers [Platt and Barr 1988] or penalty methods [Witkin et al. 1988] (i.e., "hard" or "soft" constraints). For example, simple spring forces have long been used to model joint forces and/or joint limits in the context of articulated rigid bodies [Isaacs and Cohen 1987; Wilhelms 1987]. Such an approach can be highly flexible: meshes need not even be geometrically conforming and constraints can be tailored to particular tasks. However, this strategy introduces some mesh redundancy and may be more complex than necessary for many common elastic body scenarios. Our mixed-dimensional elastic coupling energies can be interpreted as particular instances of penalty methods for enforcing coupling of coordinate frames, although the coupling of positions is guaranteed implicitly through the use of a single

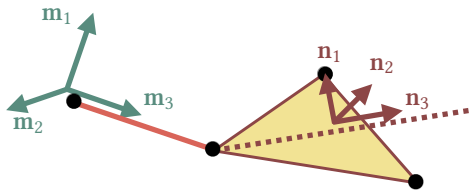

Fig. 3. A rod-shell point connection with coordinate frames. The dashed line represents the shell's twisting axis.

conforming mesh. Tournier et al. [2015] recently presented a method that conceptually unifies elasticity and constraints in order to handle constrained systems in a stable fashion; we expect that this technique could be beneficially applied alongside the elastic connection energies that we propose. Another coupling approach, related to Lagrange multipliers, is to directly "bind" or "embed" some particles such that their motion is driven strictly by that of a parent [Sifakis et al. 2007; Twigg and Kacic-Alesic 2010]; this can also be interpreted as a kind of reduced coordinate model, in that the positions of bound particles are described only in relation to their parent object's vertices or reference frame, rather than as truly independent degrees of freedom. In our unified representation, all vertices belong to a single conforming simplicial mesh, so no explicit binding is necessary.

3 POINT CONNECTIONS

We consider each of the three basic types in turn: shared point, shared curve, and shared surface. Such connections may be treated as either stiff / hard constraints, in which the initial relative orientation of the two components remains unchanged, or as soft elastic connections, which allow modeling of flexibly deforming joints. Our discussion and evaluation focuses on the latter elastic penalty-like scenario, since it enables more general deformations and introduces interesting modeling challenges. However, in the case of truly "hard" constraints, a Lagrange multiplier formulation is often preferable, so our discussions will briefly touch on this variation.

There are five cases of connections at a single point ("point connections"): rod-shell, rod-solid, shell-shell, shell-solid, and solid-solid. Despite this variety, we handle them consistently: we construct coordinate frames for each side of a connection at the shared point, and design appropriate deformation energies based on the *change* in their relative configurations. The main technical hurdle arises in accurately measuring these changes.

Since our geometry is a single conforming mesh, there is no need to explicitly enforce positional coincidence of shared vertices; their shared degrees of freedom implicitly yield ball-joint behavior in the absence of additional forces. This leaves only deviations in orientation to consider. For hard constraints, we can simply constrain the axes (or directors) of one coordinate frame to be fixed with respect to the other, by requiring fixed dot products. Denoting the two coordinate frames with their director vectors, $\{\mathbf{m}_1, \mathbf{m}_2, \mathbf{m}_3\}$ and $\{\mathbf{n}_1, \mathbf{n}_2, \mathbf{n}_3\}$ (e.g., Figure 3), we have the constraint

$$\begin{bmatrix} \mathbf{m}_1^T \\ \mathbf{m}_2^T \\ \mathbf{m}_3^T \end{bmatrix} \begin{bmatrix} \mathbf{n}_1, \mathbf{n}_2 \end{bmatrix} - \begin{bmatrix} \overline{\mathbf{m}}_1^T \\ \overline{\mathbf{m}}_2^T \\ \overline{\mathbf{m}}_3^T \end{bmatrix} \begin{bmatrix} \overline{\mathbf{n}}_1, \overline{\mathbf{n}}_2 \end{bmatrix} = \mathbf{0}. \tag{1}$$

where overlines denote rest state quantities. Constraining only two directors, $\overline{\mathbf{n}}_1$ and $\overline{\mathbf{n}}_2$, suffices because the third is orthogonal.

For softer elastic connections, a first obvious choice would be to form an elastic potential by squaring the left side of (1) and multiplying by a stiffness parameter. This is undesirable for two

reasons. First, it cannot support accumulated twisting angles that exceed π; in such a case, the joint will suddenly begin rotating in the *opposite* direction, since this is the quickest path to realigning the directors, despite the fact that it actually further *increases* the true net twist. Second, this formulation does not explicitly separate twisting and bending deformations into orthogonal modes, which implies that their stiffness parameters cannot be assigned independently. Our experience suggests that the ability to separately control bending and twisting behavior is a feature that artists find useful. Therefore, we instead seek inspiration from the dynamics of elastic rods.

3.1 Twisting energy

Twisting energy is accumulated when the two sides of a point connection become twisted with respect to their undeformed relative configurations. While a rod inherently possesses a centerline around which twisting is measured, shell and solid models do not. To ensure a compatible interface we must construct appropriate twisting axes and associated coordinate frames, but we temporarily defer this discussion to Section 3.3.

For now, consider two simplices sharing a single vertex, with associated orthonormal coordinate frames, $\{\mathbf{m}_1, \mathbf{m}_2, \mathbf{m}_3\}$ and $\{\mathbf{n}_1, \mathbf{n}_2, \mathbf{n}_3\}$, where the simplices' centerlines (rods) or chosen twisting axes (shell, solid) are assumed to lie along $\mathbf{m_3}$ and $\mathbf{n_3}$, respectively, as in Figure 3. Unfortunately, these two axes will not necessarily be mutually aligned, so the twist angle *cannot* be correctly measured by simply examining the change in angle between their perpendicular directors, $\mathbf{m}_1$ and $\mathbf{n}_1$. Instead, we adapt ideas from the elastic rods of Bergou et al. [2008],

Recall that discrete *parallel transport* applies the minimal rotation about the binormal that keeps a tangent vector tangential to the implied curve, as we move from one segment to the next. By parallel transporting the perpendicular director $\mathbf{m}_1$ into the other coordinate frame, we find a vector $\mathbf{m}_1^{PT}$ which *can* be safely compared to $\mathbf{n}_1$ to determine the actual twist angle, δ (Figure 4a). Given the angle δ, we define the point's twisting energy as

$$E_t = \frac{1}{2} k_t (\delta - \overline{\delta})^2, \tag{2}$$

where δ is the deformed angle, $\overline{\delta}$ is its undeformed counterpart, and k_t is the twisting stiffness coefficient. Since the parallel transport operation is perfectly reversible, the choice of which simplex coordinate frame to start from is arbitrary.

Remark. This energy is intentionally defined to be concentrated at the singular non-manifold point, rather than as an integral over a local region. This allows for greater consistency and flexibility for general deformable connections. Specifically, we prefer that a point connection: (1) yield consistent deformation behavior independent of the resolution (length/area/volume) of incident simplices; (2) support an arbitrary choice of stiffness independent of the incident material type(s). (By contrast, point-based models such as Elastons [Martin et al. 2010] require uniform material behavior across all (implied) dimension transitions.)

Incremental angle update. The remaining shortcoming of this approach is that if the angle deviation δ is (re-)computed directly from the coordinate frames at each step, the resulting angle (and energy) will suffer from discontinuous jumps as δ wraps around in the space of angles; for example, the relevant trigonometric functions cannot naturally distinguish π from 3π based on the current coordinate frames alone. Prior rod-only models do not typically suffer from this issue due to their choice of twist representation, such as quaternions or persistent scalar twisting angles [Bergou et al. 2008; Spillmann and Teschner 2007]. The absence of this information in general simplices necessitates our new approach.

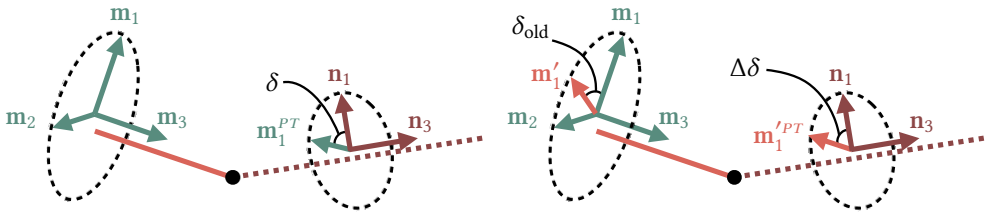

(a) Direct angle update. A subsequent post-processing step is required to ensure the correct angle increment is determined (**Incremental I**).

(b) Incremental angle update (**Incremental II**).

Fig. 4. Point connection angle updates using parallel transport.

We propose two possible incremental angle update schemes that can overcome this by instead solving for only the *incremental* change in δ, while properly accounting for parallel transport:

- **Incremental I:** After performing the direct angle update (Figure 4a), one can apply an additional post-processing step to circumvent the discontinuous angle jumps. Instead of using the computed angle directly, we first add (or subtract) the multiple of 2π that yields the closest angle to the angle from the previous time step.
- **Incremental II:** Alternatively, one can pre-rotate the director ($\mathbf{m}_1$) by the previous accumulated angle (δ_{old}), before parallel transporting to compare with the other director. Consider the twisting angle at a rod-shell connection as an example (Figure 4b). Before parallel transporting $\mathbf{m}_1$ to the other frame, we rotate $\mathbf{m}_1$ around $\mathbf{m}_3$ by δ_{old} to yield $\mathbf{m}_1'$, as shown in Figure 4b. We then apply parallel transport to get $(\mathbf{m}_1')^{PT}$, and compute the angle increment as the angle between $(\mathbf{m}_1')^{PT}$ and $\mathbf{n}_1$. This process yields an update to δ of

$$\delta = \delta_{\text{old}} + \operatorname{arctan2}((\mathbf{m}_1')^{PT} \cdot \mathbf{n}_2,\ (\mathbf{m}_1')^{PT} \cdot \mathbf{n}_1). \tag{3}$$

The above methods work equally well and share the same mild limitation: the angle increment cannot exceed π on a single timestep.

3.2 Bending energy

Bending also measures an angle deviation, but in the directions orthogonal to twisting. To calculate the bending force, we track the degree to which the second coordinate frame's twisting axis, $\mathbf{n}_3$, deviates from its rest state in the first coordinate frame. Let $\mathbf{d}$ be defined as

$$\mathbf{d} = (\mathbf{n}_3 \cdot \mathbf{m}_1, \mathbf{n}_3 \cdot \mathbf{m}_2, \mathbf{n}_3 \cdot \mathbf{m}_3) \tag{4}$$

which is simply the second frame's twisting axis $\mathbf{n}_3$ expressed in the first coordinate frame.

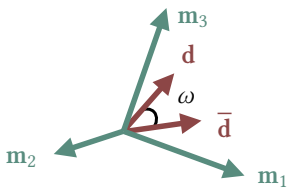

Fig. 5. Bending at a point connection. When expressed in the other coordinate frame (green) the twisting axis is denoted by $\mathbf{d}$ and compared with its rest state counterpart, $\bar{\mathbf{d}}$, to determine the bending angle ω.

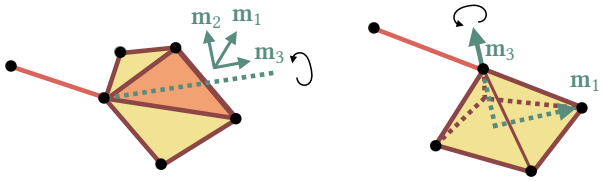

(a) Boundary point. (b) Interior point.

Fig. 6. Twisting axis $\mathbf{m}_3$ choices for a shell, at a rod-shell point connection.

The angle difference between $\mathbf{d}$ and its undeformed counterpart $\bar{\mathbf{d}}$ gives the bending angle ω, as illustrated in Figure 5. Consequently, the bending energy has the form

$$E_b = \frac{1}{2} k_b \omega^2. \tag{5}$$

We do not treat the angle update for ω incrementally because unlike twisting there is no single axis around which this bending occurs, i.e., $\mathbf{d}$ can deviate from $\bar{\mathbf{d}}$ in multiple directions.

3.3 Choosing Coordinate Frames at Vertices

Applying our twisting and bending energies at a point requires defining appropriate orthonormal coordinate frames at the shared vertex, with their third director aligned along the centerline (rods) or along an appropriately chosen twisting axis (shells and solids). For rods, the natural coordinate frame is its inherent material frame. For shells or solids, twisting axes could be chosen by the user to enable various behaviors. We suggest some natural choices below.

3.3.1 Shells. For a shell, the point connection may either be on the shell's outer boundary (Figure 6a) or in the interior (Figure 6b). For the shell boundary case, we set the twisting axis, $\mathbf{m}_3$, to be the tangent vector that bisects the total angle formed by all the incident shell triangles, in their rest configuration (Figure 6a). The triangle's normal can be used as $\mathbf{m}_1$, and the remaining vector $\mathbf{m}_2$ is determined from the cross-product of the other two.

For the shell interior case, we define the twisting axis $\mathbf{m}_3$ to be the vertex normal of the triangle mesh, which is a function of the one-ring of vertices around the point. A second director $\mathbf{m}_1$ can be found by taking one edge of an incident triangle and projecting out its component along $\mathbf{m}_3$; their cross-product provides $\mathbf{m}_2$. Using only a single edge in this can slightly bias the behavior with respect to that edge, in the sense that only changes in that edge influence $\mathbf{m}_1$ and $\mathbf{m}_2$. If this is deemed undesirable, it can be avoided by simply creating a duplicate twisting energy for each incident edge, and re-scaling the stiffness coefficients to compensate. (Since bending involves only the single $\mathbf{n}_3$ vector on one side, this issue is absent for the bending energy, except when both sides are shells or solids.)

3.3.2 Solids. For the solid case, two natural options present themselves. The first is to compute a surface vertex normal as the twisting axis, and connect it to the single tetrahedron penetrated by that vector; this is essentially a 3D extension of the shell boundary approach of Figure 6a. The second possibility is to mimic the shell interior case, where the solid's exterior triangulation takes the place of the shell triangulation. From an implementation standpoint, the former is more attractive since the stencil involves only one simplex on each side, whereas the latter involves the whole one-ring of triangles.

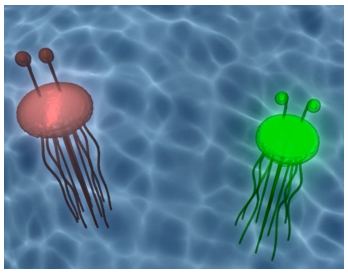

Fig. 7. **Jellyfish:** An alien jellyfish species composed of rod, shell, and solid components joined by point connections.

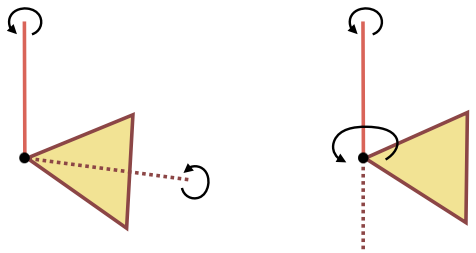

Fig. 8. Influence of twisting axis choice: when the rod is rotated, our proposed twisting axis causes the shell to rotate in a manner analogous to an elastic rod, i.e., about its own centerline (left). An alternative would be to use the rod's axis for the shell frame, which leads to different behavior (right).

Remark. The choices above yield behavior that is, by design, analogous to elastic rods in the manner in which twisting propagates between elements. While this is a natural choice, it is important to understand its effect. Consider a shell joined *at an angle* to a rod (Figure 8). Under the approach outlined above, rotating the rod will cause the shell to rotate *about its own twisting axis*, akin to elastic rods or bevel gears that meet at an angle, rather than, for example, rotating about the centerline of the rod. If the latter option were desired, one could construct the coordinate frame for the shell based on the rod, though this would be inconsistent with the behavior of regular rod-rod connections.

4 CURVE CONNECTIONS

A curve connection between two models can arise in several cases: two solids sharing a surface curve, a solid sharing a surface curve with a shell's boundary or interior, or a rod embedded within either the boundary or the interior of a shell or solid. Our assumption of a unified conforming mesh ensures that both sides of the joint share the exact same curve edges; therefore, no relative tangential sliding can occur. Furthermore, we do not need to penalize deformations of the shared curve itself, since these can be directly handled by adding a rod model, if such a behavior is desired. Therefore the only relevant deformation mode at the shared curve is relative rotation of the two sides around the curve. Our conforming mesh immediately guarantees hinge-like behavior by default; in the embedded rod case, this manifests as free rotation within its containing shell or solid, like a tent pole through a fabric sleeve (see e.g., Figure 13, middle). This can be a useful modeling choice in its own right, but if we do wish to penalize relative deformations around the edge, we need an appropriate energy. We assume that coordinate frames for each side of the joint are chosen

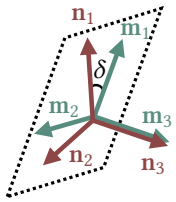

Fig. 9. Curve Connection: Two frames with axes $\mathbf{m}_3$ and $\mathbf{n}_3$ aligned along the shared edge are compared by examining the angle between $\mathbf{m}_1$ and $\mathbf{n}_1$.

such that $\mathbf{m}_3$ and $\mathbf{n}_3$ are aligned along the shared curve (unlike point connections). We defer a detailed discussion of coordinate frame construction to Section 4.2.

For a hard constraint, the relative orientation of the coordinate frame directors perpendicular to the curve should not drift over time; that is, the dot products should be constant, using

$$\begin{bmatrix} \mathbf{m}_1^T \\ \mathbf{m}_2^T \\ \mathbf{m}_3^T \end{bmatrix} \mathbf{n}_1 - \begin{bmatrix} \overline{\mathbf{m}}_1^T \\ \overline{\mathbf{m}}_2^T \\ \overline{\mathbf{m}}_3^T \end{bmatrix} \overline{\mathbf{n}}_1 = \mathbf{0}. \tag{6}$$

where again overline notation indicates rest configuration quantities. As described for point connections, however, simply squaring the left side of this expression does not provide a robust elastic energy, if we wish to support large accumulated deformations (e.g., a shell rotating around a rod by more than π radians). We therefore introduce an angle-based elastic energy to penalize relative rotational deformation between frames around a shared axis. We determine the angle δ between $\mathbf{m}_1$ and $\mathbf{n}_1$ (Figure 9) and use it to construct a quadratic energy that is integrated along the length of the shared curve. Letting $\overline{\delta}$ be the desired rest angle and k_b the stiffness of the connection, the resulting smooth energy integral is

$$\int \frac{1}{2} k_b (\delta - \overline{\delta})^2. \tag{7}$$

Similar to the point connection case, we prioritize consistency and flexibility by assigning this energy an independent stiffness parameter and concentrating it on the singular non-manifold curve. That is, the potential is integrated only along the curve's length, rather than over some local finite volume.

4.1 Discretization

Discretizing this energy along the relevant edges of our discrete simplicial mesh, we arrive at a bending-like energy that is a sum over the edges comprising the curve,

$$E_b = \sum_i \frac{1}{2} k_b \|\mathbf{e}^i\| \left(\delta^i - \overline{\delta^i}\right)^2, \tag{8}$$

where the superscript i indicates the index of the edge, and $\|\mathbf{e}^i\|$ indicates the length of the edge $\mathbf{e}^i$. It remains only to define and construct the angle δ^i. Since we assumed that $\mathbf{m}_3$ and $\mathbf{n}_3$ are mutually aligned along the shared curve, we only need to measure the angle between $\mathbf{m}_1$ and $\mathbf{n}_1$:

$$\delta = \text{arctan2}(\, \mathbf{n}_1 \cdot \mathbf{m}_2, \mathbf{n}_1 \cdot \mathbf{m}_1). \tag{9}$$

The approach above will still suffer from discontinuous jumps in angle unless an incremental approach is adopted. As described in Section 3, we have two choices of incremental update. The first approach (Incremental I) can be applied in the same way as in the point connections: calculate

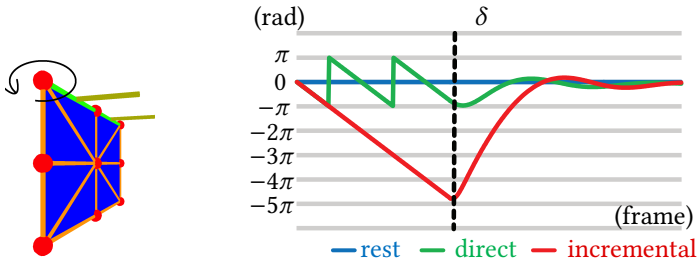

Fig. 10. A comparison between the computed angle δ using direct and incremental updates, for a green rod with a large prescribed rotational velocity embedded in a blue shell, under the given rest configuration (left). We hold the shell vertices fixed for the frames preceding the dashed line while the rod rotates to store up energy. The direct update does not capture the correct angle between the rod's material director (yellow) and the shell's normal vector, so when we release the constrained vertices (vertical dashed line), the shell does not rotate correspondingly. However, the incremental update (red) remembers the history of the deformation, and therefore the shell shows proper angular acceleration to untwist the object at the connection.

the angle δ naïvely, and then apply a post-processing step to find the true angle. To use the second approach (Incremental II), we again pre-rotate the director $\mathbf{m}_1$ with the previous angle (δ_{old}) and compare it with $\mathbf{n}_1$ to get the angle increment. This is conceptually consistent with our point connection treatment, but simpler because parallel transport is not needed.

As a concrete illustration of our incremental updates, we initialize a rod edge in a single shell triangle with the rest angle $\bar{\delta}$ set to 0 radians as shown in Figure 10, left. In the test scenario, we constrain the movement of the shell for the early frames and later release it, while the rod is prescribed to rotate with a constant angular velocity throughout. We observe the values of δ as we rotate the rod while applying the elastic forces described above. As in Figure 10, right, we see that the direct angle updates (green curve) show unphysical sudden jumps and they are also unaware of the accumulated bending angle (i.e. 3π deformation is regarded as π). By contrast, our incremental update (red curve) exhibits smooth changes in δ and it tracks the complete angular deformation.

4.2 Choosing Coordinate Frames at Edges

The coordinate frame for a rod is simply its material frame; $\mathbf{m}_3$ is the vector along the (shared) centerline curve. For shells, a coordinate frame can be constructed by setting $\mathbf{m}_3$ as the unit tangent vector along the shared edge. We define $\mathbf{m}_1$ as the normal vector at the edge, which may be either the normal of a single triangle for shell boundary edges, or the average normal of two incident triangles for interior edges. The cross-product yields $\mathbf{m}_2$.

For solids, there are two situations to consider. First, for a solid with an embedded rod, we construct an independent energy for each triangle from the set of tetrahedra incident on the shared edge to minimize bias that would arise in coupling only a single rod-tetrahedron pair. As such, the necessary coordinate frames are constructed for each individual triangle in the same manner as for the shell boundary case above. Second, for a solid sharing a surface curve with a shell or another solid, we use the exterior surface triangulation to construct the coordinate frame, as we did for the interior case of the shell. That is, $\mathbf{m}_3$ lies along the edge, $\mathbf{m}_1$ is the average edge normal from the two incident triangles, and the cross-product is again used to find $\mathbf{m}_2$.

5 SURFACE CONNECTIONS

The final case, in which two different models share a surface, arises only when a shell is embedded within or on the surface of a solid object. The shell imposes its additional stretching, shearing,

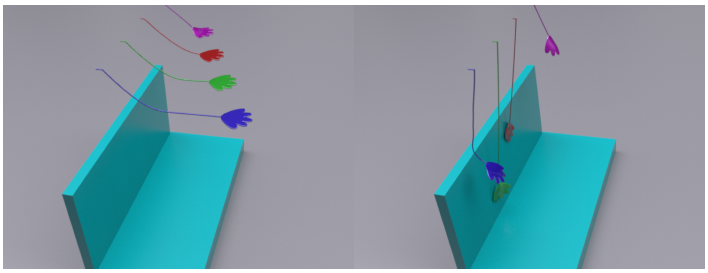

Fig. 11. **Sticky Hands:** Rubber children's toys modeled as non-manifold meshes comprised of rod and shell components.

and bending forces on the surface shared with the solid. Since our framework assumes a single conforming mesh (without sliding), this type of connection is trivial: we label the appropriate simplices as standard shell or solid elements, and apply their associated forces to the vertices as usual. Unlike point or curve connections, no remaining degrees of freedom exist.

6 RESULTS

Our animation examples were computed on a 2.8 GHz Intel Core i7 processor. Single-threaded performance data is listed in Table 1; however, there likely remain significant opportunities for optimizing our prototype implementation, as our focus is primarily on the flexibility of the system rather than speed. Moreover, since cross-dimensional connections typically comprise a small subset of the domain compared to single-type regions, our modifications are unlikely to be a bottleneck unless the elastic coupling is far stiffer than the surrounding material.

Each example is constructed by first designing a single non-manifold geometric mesh, and then tagging simplices and simplex-pairs with model types and connection types, respectively. We employed Bridson's collision detection and resolution strategy [Bridson et al. 2002]. Time integration was performed with backward Euler; we solved the resulting nonlinear systems using a standard Newton solver with conjugate gradient for the inner linear solves, although it would be interest to explore alternatives for greater efficiency [Li et al. 2019]. We did not observe any significant change in the stability using our method as compared to pure simulations of a particular dimension. Our model is agnostic to the topology of the simulated object, so loops in the graph of connected components likewise have no discernible effect on stability.

Didactic Examples. Our supplemental video includes several animations that exercise the various connection types in isolation. For each connection type, a scenario is shown with and without the associated energy being applied, in order to highlight the behavior that it assigns to the simplicial mesh. Figure 2 shows a scenario where a single complex non-manifold simplicial mesh is assigned many individual connection types. In the video, the tetrahedron on the right end is scripted to rotate, leading the entire shape to rotate, bounce, and deform elastically.

Toy Ball. In the basic example of Figure 12, a single mesh is used to represent three distinct components that have been point-connected together: rod (spring), shell (platform/suction cup), and solid (ball). The result is a springy-ball toy.

Sticky Hands. The sticky hand toy example of Figure 11 shows an elastic object composed of a single material featuring rod-like and shell-like parts joined through stiff point connections.

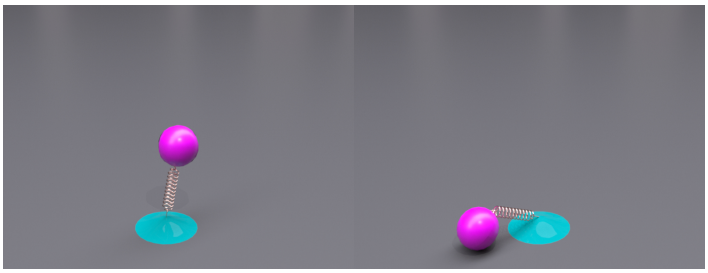

Fig. 12. **Toy Ball:** A ball-and-spring toy composed of three point-connected parts. The behavior is very different with proper point connection energies in comparison with the one without any coupling energies (right).

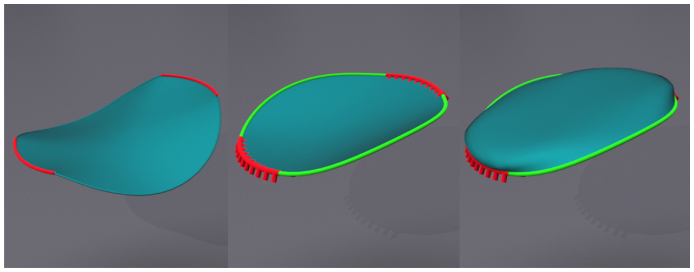

Fig. 13. **Nylon Frisbee:** A circular frisbee composed of a shell with different rod embeddings along its boundary. We prescribe an axial rotation of two sides of the boundary curve (red), and observe the resulting behavior. Left: Without a rod. Middle: With a rotationally uncoupled embedded rod. Right: With a rotationally coupled embedded rod.

Jellyfish. Our alien jellyfish example (Figure 7) consists of components of various dimensions representing the tentacles, eye stalks, eyeballs, and thin body of the jelly fish. To animate it, we prescribe the motion of the body, and allow the various appendages to deform freely.

Nylon Frisbee. Our nylon frisbee model (Figure 13) is comprised of a shell with stiff rubber rim (rod), to illustrate three distinct possible behaviors designed by decorating a simple circular mesh geometry with different materials and connections. We rotate the red region of the rod, and observe the effect of the rod on the interior cloth. In the absence of the rod, the shell hangs limply (left). With the rod added but not rotationally coupled to the cloth (middle), the rod can freely rotate so that the only effect on the cloth is through the deformation induced along the free section of the rod. With our rotational coupling added (right), the rod is instead glued to the cloth such that its rotation induces direct (bulging) deformations on the connected cloth, as expected.

Toy Tunnel. In Figure 14 we construct a children's toy tunnel from a cylindrical cloth (shell) mesh by labeling a subset of its existing edges as connected rods in a spiral pattern. Compared to a piece of pure cloth, the version with embedded rods clearly better captures the desired spring-like behavior.

Umbrella. Figure 15 shows a rendered umbrella, and a separate visualization of the rod edges of the umbrella alone. Here we see that in addition to embedded rods through the umbrella's cloth shell, the rod structure itself also contains non-manifold triple-joints, which our framework supports straightforwardly.

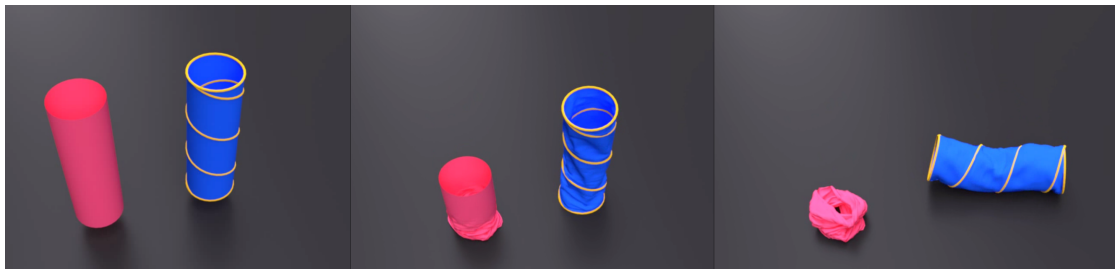

Fig. 14. **Toy Tunnel:** A falling cylindrical triangle mesh behaves very differently with its elements labeled as pure cloth (pink) as compared to cloth with embedded rod segments (blue and yellow).

Fig. 15. **Umbrella:** An umbrella closed, open, and shown with only the wireframe rod-edges rendered. The rod sub-component of the mesh contains non-manifold triple-junctions.

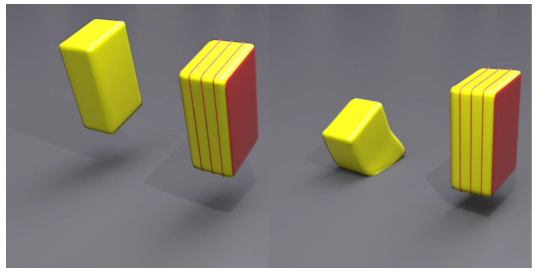

Fig. 16. **Sandwich composite:** By identifying several layers of faces within the tetrahedral mesh as stiff shells, the two same volumetric solids present totally different behaviors.

Sandwich Composite. Figure 16 shows the effect of stiff shells embedded within a softer solid volume, by labeling several layers of the tetrahedral mesh's interior triangular faces to be stiff shells.

Anglerfish. Our cartoon anglerfish example of Figure 17 contains both point connections and curve connections. The body of the anglerfish is composed of 3D tetrahedra, while fins (2D) and an antenna (1D) are connected to the body forming a curve connection and a point connection, respectively. At the end of the antenna, a light-emitting ball (3D) is attached via another point connection.

Continuous Uniform Objects. While we focus on more arbitrary elastic connections, our framework can also plausibly model smoothly continuous objects consisting of a single material. For

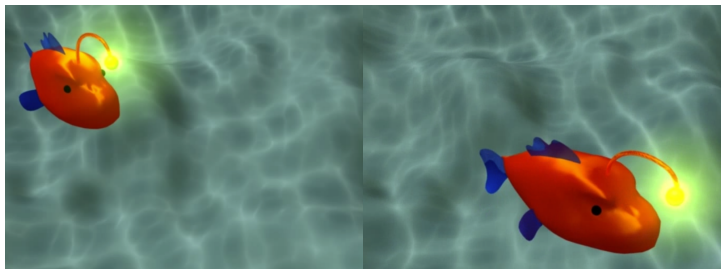

Fig. 17. **Anglerfish:** The anglerfish model is composed of 3D tetrahedra (body, light ball), 2D triangles (fins), and 1D rods (antenna) connected by both point and curve connections. The head motion is prescribed and the rest of the body's motion is induced by our elastic energies.

Scene	#vertices	#rod edges	#shell faces	#tetrahedra	#frames	Total time (s)
Toy ball	229	203	96	226	1300	218.301
Sticky hands (purple)	200	19	292	-	1000	115.605
Sticky hands (red)	200	19	292	-	1000	200.095
Sticky hands (green)	200	19	292	-	1000	212.095
Sticky hands (blue)	200	19	292	-	2000	221.073
Jellyfish (single)	1465	1273	-	454	200	528.271
Nylon frisbee	289	64	512	-	700	24.8301
Umbrella	3168	198	6144	-	600	4364.83
Sandwich composite	395	-	1510	600	5000	1311.2

Table 1. Simulation Statistics

example, if a thick solid block gradually narrows to become quite thin, at some point along its length it might be better represented as a thin shell with identical Lamé parameters.

This can be conveniently done by ensuring that the connection point/curve has no discontinuous kink in the implied continuous geometry; i.e., the point connection twisting axes or curve connection planes are aligned on both sides. We treat this with a high stiffness connection so that the components' relative configurations remain essentially unchanged (this contrasts with the softer elastic joints with potentially non-zero rest angles used elsewhere). This amalgamates the two incident elements into a smoothly interfacing *super-element*. While this yields a "flat" connection, it is no different than a flat triangle; both their regions of influence naturally shrink under refinement to approximate smooth behavior. (For a coarse mesh, if the resulting "flat" region is deemed too large relative to the surrounding elements, the two elements comprising this super-element could simply be modeled as half the size). In addition to simplicity, an advantage of this approach is that while the material parameters and thickness/diameter of each single-type model must be set to correspond, there is no need to tune the connection's stiffness parameter to precisely match as well; it is simply acting as a strong penalty constraint rather than an elastic energy.

Of course, if an elastic object is simulated with models of different dimensions (i.e., a thin solid object can be treated as either a 3D solid model with a small thickness or a 2D shell model), they might not behave perfectly consistently, depending on the choice of the single-type physical models,

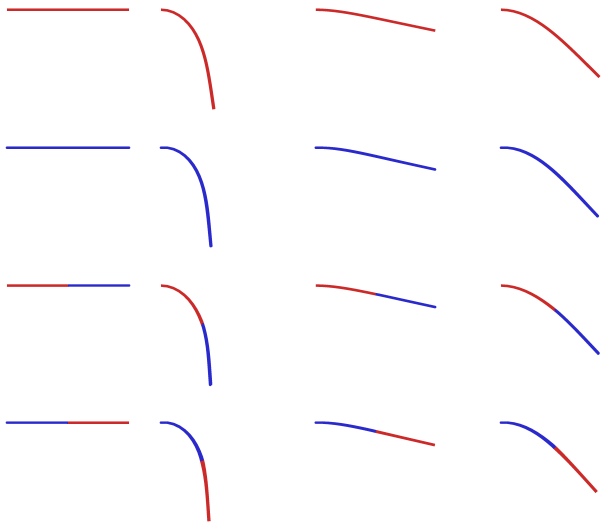

Fig. 18. Comparison between single- and mixed-dimensional models (red: solid model, blue: shell model). From top to bottom, pure 3D solid model, pure 2D shell model, half solid(left)-half shell(right) model, half shell(left)-half solid(right) model. Our method smoothly connects two different-dimensional models of the same material while preserving uniform behavior.

their discretizations, and/or the level of mesh refinement. However, as long as the two separate models have matching behaviors, connecting them with the method above does not damage the apparent homogeneity of the material. In Figure 18 we simulate a thin solid object with a 3D solid model, 2D shell model, and combinations of the two models by connecting the two half-length models with high stiffness.

7 CONCLUSIONS

We have presented an expressive and practical approach for designing and simulating diverse non-manifold and mixed-dimensional elastic objects that effectively leverages well-studied continuum models of single-dimensional elastica. The user simply models an object's desired geometry with a single conforming possibly non-manifold simplicial mesh, and then labels its simplices with model and connection types to achieve the desired target behavior.

Our assumption of a conforming mesh limits us to situations in which the two sides of a connection (or the connection itself) cannot slide relative to the bodies. In previous work, Chentanez et al. [2009] explored a method to allow a Lagrangian rod to slide while constrained within a tetrahedral mesh, and Weidner et al. [2018] enabled smooth sliding of Lagrangian cloth relative to contact points; these and related Eulerian-on-Lagrangian simulation concepts [Fan et al. 2013] may prove useful in tackling this challenge. The conforming mesh assumption also disallows connections in the interior of an element, such as a rod endpoint joined at the middle of a shell triangle.

We adopted three specific single-type elastic models for rods, shells, and solids. We expect that other options would integrate equally well, since our coupling connections place few limits on the chosen models beyond requiring simplicial meshes. Similarly, extending the single-type models with additional features or constitutive laws (e.g. strain limiting, incompressibility, plasticity) would

be largely orthogonal to the proposed approach. However, designing connections which themselves have exotic elastoviscoplasticity or angle limits may be interesting to consider in future.

Another exciting avenue to explore is the extension of our framework to mixed-dimensional *liquids*, analogous to work on viscous sheets and threads [Batty et al. 2012; Bergou et al. 2010]. While non-manifold simplicial liquid models have been suggested [Zhu et al. 2015, 2014], an approach along the lines of our framework could naturally support the characteristic twisting and bending forces (and associated buckling and coiling effects) of viscous and non-Newtonian sheets and threads, which Zhu et al. omitted. Naturally this would require incorporating mixed-dimensional dynamic remeshing, as Zhu et al. [2014] have previously demonstrated.

Despite the attractive simplicity of our point, curve, and surface connections and the commonality among the various energies, the construction of appropriate coordinate frames near connections nevertheless involves special cases that depend on the particular configuration. It is interesting to consider whether it may be possible to find an even more concise set of "atomic" stencils or energies that can be re-assembled to recover all possible models and couplings, thereby further streamlining the methodology. Finally, our approach also reveals some user interface challenges: geometric modeling tools for general non-manifold objects are less well-studied than for surface meshes, and achieving the desired deformation behavior by tagging simplices with model and connection types remains a somewhat labor-intensive process.

ACKNOWLEDGMENTS

This work was supported in part by the Natural Sciences and Engineering Research Council of Canada (RGPIN-04360-2014). We would like to thank SideFX Software for Houdini licences, and anonymous reviewers for their insightful feedback.

REFERENCES

Christopher Batty, Andres Uribe, Basile Audoly, and Eitan Grinspun. 2012. Discrete viscous sheets. *ACM Trans. Graph. (SIGGRAPH)* 31, 4 (2012), 113.

G. Beer. 1985. An isoparametric joint/interface element for finite element analysis. *Internat. J. Numer. Methods Engrg.* 21, 4 (1985), 585–600.

Miklos Bergou, Basile Audoly, Etienne Vouga, Max Wardetzky, and Eitan Grinspun. 2010. Discrete viscous threads. *ACM Trans. Graph. (SIGGRAPH)* 29, 4 (2010), 116.

Miklos Bergou, Max Wardetzky, Stephen Robinson, Basile Audoly, and Eitan Grinspun. 2008. Discrete elastic rods. *ACM Trans. Graph. (SIGGRAPH)* 27, 3 (2008), 63.

Florence Bertails, Basile Audoly, Marie-Paule Cani, Frédéric Leroy, Bernard Querleux, and Jean-Luc Lévêque. 2006. Super-helices for predicting the dynamics of natural hair. *ACM Trans. Graph. (SIGGRAPH)* 25, 3 (jul 2006), 1180–1187. https://doi.org/10.1145/1141911.1142012

Robert Bridson, Ronald Fedkiw, and John Anderson. 2002. Robust treatment of collisions, contact and friction for cloth animation. *ACM Trans. Graph. (SIGGRAPH)* 21, 3 (2002), 594–603.

Nuttapong Chentanez, Ron Alterovitz, Daniel Ritchie, Lita Cho, Kris K. Hauser, Ken Goldberg, Jonathan R. Shewchuk, and James F. O'Brien. 2009. Interactive simulation of surgical needle insertion and steering. *ACM Trans. Graph. (SIGGRAPH)* 28, 3 (2009), 88.

Fehmi Cirak and Quan Long. 2011. Subdivision shells with exact boundary control and non-manifold geometry. *Int. J. Numer. Methods Eng.* 88, 9 (2011), 897–923.

Ye Fan, Joshua Litven, David I. W. Levin, and Dinesh K. Pai. 2013. Eulerian-on-Lagrangian simulation. *ACM Trans. Graph. (SIGGRAPH)* 32, 3 (2013), 22.

François Faure, Benjamin Gilles, Guillaume Bousquet, and Dinesh K. Pai. 2011. Sparse meshless models of complex deformable solids. *ACM Trans. Graph. (SIGGRAPH)* 30, 4 (2011), 73.

Benjamin Gilles, Guillaume Bousquet, François Faure, and Dinesh K. Pai. 2011. Frame-based elastic models. *ACM Trans. Graph.* 30, 2 (2011), 15.

Yotam Gingold, Adrian Secord, Jefferson Y. Han, Eitan Grinspun, and Denis Zorin. 2004. *A discrete model for inelastic deformation of thin shells.* Technical Report. New York University. 12 pages.

Eitan Grinspun, Anil N. Hirani, Peter Schröder, and Mathieu Desbrun. 2003. Discrete shells. In *Symposium on Computer Animation*. Eurographics Association, 62–67.

Paul M Isaacs and Michael F Cohen. 1987. Controlling dynamic simulation with kinematic constraints. *ACM SIGGRAPH* 21, 4 (1987), 215–224.

T. Kugelstadt and E. Schömer. 2016. Position and orientation based Cosserat rods. In *Symposium on Computer Animation*. 169–178.

Faming Li, Xiaowu Chen, Lin Wang, and Qinping Zhao. 2014. Canopy-frame interactions for umbrella simulation. *Computers and Graphics* 38 (2014), 320–327.

Minchen Li, Ming Gao, Timothy Langlois, Chenfanfu Jiang, and Danny M. Kaufman. 2019. Decomposed Optimization Time Integrator for Large-Step Elastodynamics. *ACM Trans. Graph. (SIGGRAPH)* 31 (2019).

Miles Macklin, Matthias Müller, Nuttapong Chentanez, and Tae-Yong Kim. 2014. Unified particle physics for real-time applications. *ACM Trans. Graph. (SIGGRAPH)* 33, 4 (2014), 153.

Sebastian Martin, Peter Kaufmann, Mario Botsch, Eitan Grinspun, and Markus Gross. 2010. Unified simulation of elastic rods, shells, and solids. *ACM Trans. Graph. (SIGGRAPH)* 29, 4 (2010), 39.

Matthias Müller and Nuttapong Chentanez. 2011. Solid simulation with oriented particles. *ACM Trans. Graph. (SIGGRAPH)* 30, 4 (2011), 92.

Matthias Müller, Bruno Heidelberger, Marcus Hennix, and John Ratcliff. 2007. Position based dynamics. *Journal of Visual Communication and Image Representation* 18, 2 (2007), 109–118.

James F. O'Brien and Jessica K. Hodgins. 1999. Graphical modeling and animation of brittle fracture. In *SIGGRAPH*. ACM Press/Addison-Wesley Publishing Co., 137–146.

Jesús Pérez, Miguel A. Otaduy, and Bernhard Thomaszewski. 2017. Computational design and automated fabrication of kirchhoff-plateau surfaces. *ACM Trans. Graph. (SIGGRAPH)* 36, 4 (jul 2017), 1–12. https://doi.org/10.1145/3072959.3073695

Jesús Pérez, Bernhard Thomaszewski, Stelian Coros, Bernd Bickel, José A. Canabal, Robert Sumner, and Miguel A. Otaduy. 2015. Design and Fabrication of Flexible Rod Meshes. *ACM Trans. Graph.* 34, 4, Article 138 (July 2015), 12 pages. https://doi.org/10.1145/2766998

John C Platt and Alan H Barr. 1988. Constraint methods for flexible models. *SIGGRAPH* 22, 4 (1988), 279–288.

Olivier Rémillard and Paul G. Kry. 2013. Embedded thin shells for wrinkle simulation. *ACM Trans. Graph. (SIGGRAPH)* 32, 4 (2013), 50.

J. C. J. Schellekens and René De Borst. 1993. On the numerical integration of interface elements. *Internat. J. Numer. Methods Engrg.* 36, 1 (1993), 43–66.

Eftychios Sifakis, Tamar Shinar, Geoffrey Irving, and Ron Fedkiw. 2007. Hybrid simulation of deformable solids. In *Symposium on Computer Animation*. 81–90.

Jonas Spillmann and Matthias Teschner. 2007. CORDE: Cosserat rod elements for the dynamic simulation of one-dimensional elastic objects. In *Symposium on Computer Animation*. 63–72.

Jonas Spillmann and Matthias Teschner. 2009. Cosserat nets. *IEEE TVCG* 15, 2 (2009), 325–338.

Jos Stam. 2009. Nucleus: Towards a unified dynamics solver for computer graphics. In *Computer-Aided Design and Computer Graphics*. 1–11.

Maxime Tournier, Matthieu Nesme, Benjamin Gilles, and Francois Faure. 2015. Stable constrained dynamics. *ACM Trans. Graph. (SIGGRAPH)* 34, 4 (2015), 132.

Christopher D. Twigg and Zoran Kacic-Alesic. 2010. Point cloud glue: Constraining simulations using the Procrustes transform. In *Symposium on Computer Animation*. 45–54.

Nobuyuki Umetani, Ryan Schmidt, and Jos Stam. 2014. Position-based elastic rods. , 21–30 pages. https://dl.acm.org/citation.cfm?id=2849522

Nicholas J. Weidner, Kyle Piddington, David I. W. Levin, and Shinjiro Sueda. 2018. Eulerian-on-lagrangian cloth simulation. *ACM Trans. Graph. (SIGGRAPH)* 37, 4 (jul 2018), 1–11. https://doi.org/10.1145/3197517.3201281

Jane Wilhelms. 1987. Using dynamic analysis for realistic animation of articulated bodies. *IEEE Computer Graphics and Applications* 7, 6 (1987), 12–27.

Andrew Witkin, Kurt Fleischer, and Alan Barr. 1988. Energy constraints on parameterized models. In *SIGGRAPH*. 225–232.

Hongyi Xu, Espen Knoop, Stelian Coros, and Moritz Bächer. 2018. Bend-it: Design and Fabrication of Kinetic Wire Characters. *ACM Trans. Graph.* 37, 6, Article 239 (Dec. 2018), 15 pages. https://doi.org/10.1145/3272127.3275089

Bo Zhu, Minjae Lee, Ed Quigley, and Ronald Fedkiw. 2015. Codimensional non-Newtonian fluids. *ACM Trans. Graph. (SIGGRAPH)* 34, 4 (2015), 115.

Bo Zhu, Ed Quigley, Matthew Cong, Justin Solomon, and Ronald Fedkiw. 2014. Codimensional surface tension flow on simplicial complexes. *ACM Trans. Graph. (SIGGRAPH)* 33, 4 (2014), 111.